Quantum Electronics **41** (5) 441 – 446 (2011)

INTERACTION OF LASER RADIATION WITH MATTER

PACS numbers: 89.75.Fb; 81.16.-c; 62.23.St; 68.35.Fx; 81.40.Lm
DOI: 10.1070/QE2011v041n05ABEH014489

CW laser-induced generation of periodic ring structures on thin PbSe films

A.A. Antipov, S.M. Arakelyan, V.I. Emel'yanov, S.P. Zimin,
S.V. Kutrovskaya, A.O. Kucherik, V.G. Prokoshev

***Abstract*. Laser processing of epitaxial PbSe films has been found to produce periodic concentric surface ring structures that extend over several laser spot radii from the exposed zone. The proposed theoretical interpretation of this effect in terms of defect – deformation interactions adequately describes the observed morphology, periodicity and complex (multimode) shape of the ring structures.**

Keywords: *epitaxial semiconductor films, laser modification, defect – deformation instability*.

1. Introduction

A nanostructured state of the narrow-gap semiconductors PbSe (band gap $E_g = 0.29$ eV), PbTe (0.32 eV) and PbS (0.41 eV) is of interest for gaining insight into quantum size effects in relatively large systems, tens of nanometres in dimensions [1]. Nanostructures based on PbTe, PbSe, PbS and their solid solutions can be produced by a variety of techniques [1 – 3], including laser and laser-plasma deposition processes, which are of practical importance. Both below-band-gap ($\hbar\omega < E_g$) and above-band-gap ($\hbar\omega > E_g$) laser radiation, in different modes (e.g., laser ablation and/or heating), effectively changes the structural and electrical properties of the lead chalcogenides, producing micro- and nanostructures [4, 5]. This paper examines a new effect: generation of concentric periodic surface ring structures that extend over several laser spot radii from the directly exposed zone. Such structures result from cw laser processing of epitaxial lead selenide films at $\lambda = 1.06$ μm ($\hbar\omega > E_g$).

2. Experimental

PbSe/CaF_2/Si(111) heterostructures were grown by molecular-beam epitaxy at the ETH Zurich. The thickness of the PbSe film was varied from 0.3 to 4 μm. The CaF_2 buffer was 2 – 4 nm in thickness and served to compensate for the lattice mismatch between the silicon substrate and epitaxial film. The lead selenide layer was single-crystal, with its (111) plane normal to the growth direction. The structural parameters of the films were reported elsewhere [6].

The experimental setup used for laser irradiation was described earlier [7 – 9]. A Nd : YAG laser beam (LS-02-T laser, 5 to 15 W output power, $\lambda = 1.06$ μm) was focused to a spot diameter of 30 μm on the sample surface. The incident power density was thus 10^4 to 10^5 W cm^{-2}. During the laser exposure, the sample was scanned with the laser beam on a positioning stage, which was translated at 80 μm s^{-1}. The laser-exposed zone on the sample surface was examined in real time using a laser monitor, which allowed us to directly control the exposure conditions. Figure 1 presents typical instantaneous images of laser-exposed surfaces in the solid-state and liquid-phase target modification regimes. Solid-state modification (Fig. 1a) is accompanied by a characteristic change in the reflectance of the sample surface (5-W laser output). In the top right of the image, there is a laser beam trace on the sample surface. The trace is 30 μm in width, which corresponds to the laser spot diameter on the sample surface.

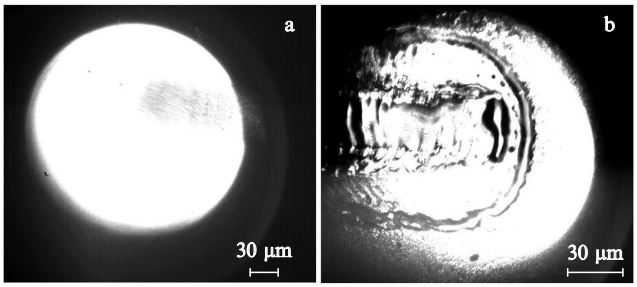

Figure 1. Instantaneous images of laser-exposed PbSe surfaces (real-time examination using a laser monitor): (a) solid-state modification (incident power, 5 W); (b) molten surface (incident power, 15 W).

In the liquid-phase modification regime (Fig. 1b), involving laser-induced surface melting (15-W power), we observe a qualitatively different picture. Laser heating induces circular surface perturbation (of the order of 3 μm in width), which propagates away from the centre of the zone under irradiation. Traces of the ejected material are seen in the image. At a distance of the order of the laser spot radius, another perturbation emerges on the film surface (of the same thickness) and travels in front of

A.A. Antipov, S.M. Arakelyan, S.V. Kutrovskaya, A.O. Kucherik, V.G. Prokoshev Vladimir State University, ul. Gor'kogo 87, 600000 Vladimir, Russia; e-mail: AAntipov@vlsu.ru, arak@vlsu.ru, KStella@vlsu.ru, kucheric@vlsu.ru;
V.I. Emel'yanov Department of Physics, M.V. Lomonosov Moscow State University, Vorob'evy gory, 119991 Moscow, Russia; e-mail: emelyanov.vladimir@gmail.com;
S.P. Zimin P.G. Demidov Yaroslavl State University, Sovetskaya ul. 14, 150000 Yaroslavl, Russia

Received 12 November 2010; revision received 13 January 2011
Kvantovaya Elektronika **41** (5) 441 – 446 (2011)
Translated by O.M. Tsarev

the laser beam. Between these two perturbations are separate droplets up to 2 μm in radius.

Figure 2 shows the surface of a $PbSe/CaF_2/Si$ sample after two sequential exposures to 5-W cw laser radiation in the solid-state modification regime (2-μm-thick PbSe film). The surface image was obtained on a Ntegra-Aura atomic force microscope in intermittent contact mode. During the first exposure of the sample surface, the centre of the laser spot was in the top left corner of the image. Before the second exposure, the sample was displaced so that the centre of the laser spot was in the bottom left corner during the second exposure. Both exposures produced a periodic ring structure on the surface around the centre of the laser spot (in Fig. 2, the two centres of the exposed zones associated with the displacement of the sample are connected by a dark band due to the laser exposure). The laser-induced surface structure extends over a distance of ~ 50 μm, that is, beyond the laser spot (~ 15 μm). The surface profile is highly nonuniform (Fig. 3), with strong peaks 10 – 14 μm apart, which is about twice their width. The roughness height decreases with increasing distance from the centre of the laser spot.

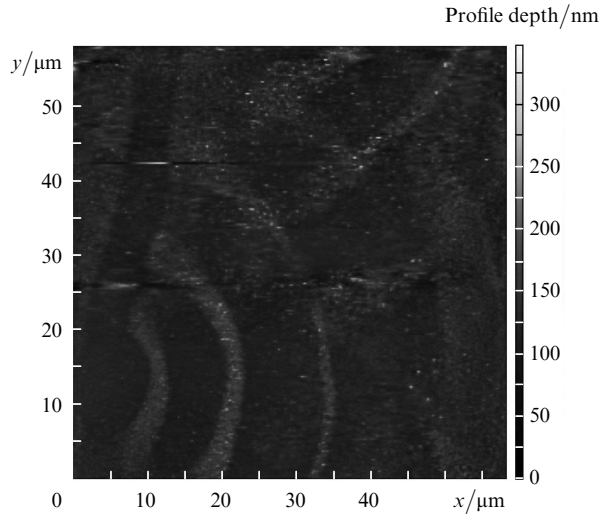

Figure 2. Atomic-force microscope image of a PbSe surface after laser exposure (5-W power).

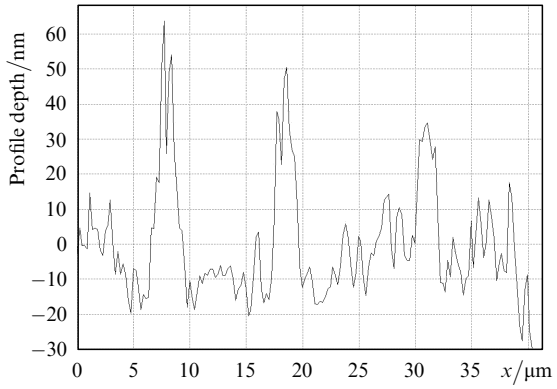

Figure 3. Observed nonuniform surface profile corresponding to a ring structure with its centre in the bottom left corner of Fig. 2.

3. Defect – deformation mechanism of ring structure formation

We describe the observed effect in terms of a film model for defect – deformation (DD) instability [10, 11], generalising it to axisymmetric systems. Consider a PbSe film of thickness h on a CaF_2/Si substrate. Laser radiation heats it within the laser spot and in the surrounding region of radius equal to the thermal diffusion length, $r_T = (\chi\tau_L)^{1/2}$, where $\chi \sim 0.1$ cm^2 s^{-1} and $\tau_L \sim 0.2$ s are the thermal diffusivity and exposure time, respectively. For $r_T > h$, the film is heated throughout its thickness and has the form of an axisymmetric membrane in the elevated-temperature region.

Laser heating causes the Pb and Se atoms in the heated zone to leave their lattice sites, thereby producing vacancies. This leads to active vaporisation of surface atoms, formation of excess vacancies in the near-surface region, and accelerated diffusion and drift of interstitials from the bulk to the surface. Vacancies in turn drift against the temperature gradient (thermal strain gradient), i.e., from the surface to the bulk of the film. This produces an increased concentration of nonequilibrium vacancies in the bulk of the heated membrane and excess interstitials on its surface.

Lead chalcogenide films on Si(111) with a CaF_2 buffer are known to be in a tensile state in the plane of the film [6, 12]; i.e., the film is under tensile stress, $\sigma_{\|} > 0$. Assume that laser heating does not change the sign of $\sigma_{\|}$, which is favoured by the high vacancy concentration in the film.

Above a critical defect density, the stressed (tensile) surface membrane saturated with mobile point defects is unstable and passes into an axisymmetric, periodically bent steady state, with defect accumulation at extrema in the surface profile of the membrane. The spatial distribution of the static strain in the membrane is specified in the same way as that in Lamb dynamic bending waves in plates [13]. Such a periodically modulated surface profile with the associated defect accumulation grating constitutes an axisymmetric surface DD ring structure, which can be characterised by its wavenumber q. A DD structure results from the development of a DD instability. In its linear regime, the amplitude of ring structures increases over time as $\exp(\lambda_q t)$, where λ_q is the growth rate. The value $q = q_m$ at which the growth rate reaches a maximum determines the period of predominant ring structures, $\Lambda_m = 2\pi/q_m$, which stand out in the Fourier spectrum of the surface profile.

In a nonlinear regime, the axisymmetric system of DD equations derived in this study describes three-wave interactions of DD ring structures (in particular, surface-profile second harmonic generation, with a wavenumber $2q$, and third DD harmonic cascade generation, with a wavenumber $3q$), like in a previous study [14]. The present results demonstrate that a superposition of the first to fourth DD ring harmonics ensures a sufficiently good description of the observed ring profile resulting from laser irradiation of the sample surface.

4. Equations describing a DD instability of a stressed circular membrane containing mobile point defects

Consider a tensile circular PbSe film (membrane) of thickness h, containing a concentration n_d of point defects (interstitials and vacancies): $n_d = n_v$ for vacancies and $n_d = n_i$ for interstitials. Let the $z = 0$ plane coincide with

the film surface and the z axis be directed from the surface to the bulk of the sample.

The defect distribution in the film can be written in the form

$$n_{\mathrm{d}}(r,z,t) = N_{\mathrm{d}}(r,t)f(z), \tag{1}$$

where $N_{\mathrm{d}}(r,t)$ is the defect density in the $z=0$ plane; r is the in-plane distance from the centre of the laser spot; and the function $f(z)$ defines the defect distribution along the normal to the film and will be determined below [see (12)].

In deriving the constitutive equations of this model, we take the surface diffusion and defect drift to be isotropic. The lateral surface flux of defects, $\boldsymbol{j}_{\mathrm{d}}$, comprises diffusion and deformation terms:

$$\boldsymbol{j}_{\mathrm{d}} = -D_{\mathrm{d}}\nabla N_{\mathrm{d}} + N_{\mathrm{d}}\frac{D_{\mathrm{d}}}{kT}\boldsymbol{F}(r). \tag{2}$$

Here D_{d} is the surface diffusion coefficien;

$$\boldsymbol{F}(r) = \theta_{\mathrm{d}}\nabla(\xi)_{z=0} \tag{3}$$

is the lateral force acting on a defect from the deformed elastic continuum of the membrane;

$$\nabla = \frac{\boldsymbol{e}_{\mathrm{r}}}{r}\frac{\mathrm{d}}{\mathrm{d}r}(r)$$

is the lateral gradient; $\boldsymbol{e}_{\mathrm{r}} = \boldsymbol{r}/r$ is a unit vector; $\theta_{\mathrm{d}} = \Omega_{\mathrm{d}}K$ is the deformation potential of the defect; Ω_{d} is the volume change upon the formation of one defect; K is the elastic modulus; $\xi = \xi(r,z) = \mathrm{div}\boldsymbol{u}$ is the strain in the membrane; $\boldsymbol{u} = \boldsymbol{u}(r,z,t)$ is the displacement vector of points in the membrane; k is the Boltzmann constant; and T is the absolute temperature.

Substituting (3) into the continuity equation for N_{d}, we obtain an equation of surface diffusion which takes into account the deformation-induced defect drift:

$$\frac{\partial N_{\mathrm{d}}}{\partial t} = D_{\mathrm{d}}\Delta N_{\mathrm{d}} - \frac{D_{\mathrm{d}}\theta_{\mathrm{d}}}{kT}\,\mathrm{div}[N_{\mathrm{d}}\nabla(\xi)]_{z=0}, \tag{4}$$

where

$$\Delta = \frac{1}{r}\frac{\partial}{\partial r}\left(r\frac{\partial}{\partial r}\right)$$

is the lateral Laplacian; and

$$\mathrm{div}\boldsymbol{A} = \frac{1}{r}\frac{\mathrm{d}}{\mathrm{d}r}(r\boldsymbol{A}\cdot\boldsymbol{e}_{\mathrm{r}}).$$

The strain of the film, $\xi = \mathrm{div}\boldsymbol{u}$, is given by [15]

$$\xi(r,z,t) = -v\left(z-\frac{h}{2}\right)\Delta\zeta(r,t), \tag{5}$$

where $v = (1-2\sigma_{\mathrm{p}})/(1-\sigma_{\mathrm{p}})$; σ_{p} is the Poisson's ratio of the film; and ζ is the bending coordinate of the film (displacement of the points in the median plane along the z axis). The linear, sign-alternating variation of the strain in the film with z, represented by (5), is a characteristic feature of Lamb waves in plates [13].

Substituting (5) into (4), we obtain

$$\frac{\partial N_{\mathrm{d}}}{\partial t} = D_{\mathrm{d}}\Delta N_{\mathrm{d}} - \frac{vhD_{\mathrm{d}}\theta_{\mathrm{d}}}{2kT}\,\mathrm{div}[N_{\mathrm{d}}\nabla(\Delta\zeta)]. \tag{6}$$

For ζ, we can write the linear equation [11]

$$\frac{\partial^2\zeta}{\partial t^2} + l_0^2c^2\Delta^2\zeta - \frac{\sigma_{\parallel}}{\rho}\Delta\zeta = \sum_d\left\{\frac{\theta_{\mathrm{d}}}{\rho h}\int_0^h\frac{\partial n_{\mathrm{d}}}{\partial z}\,\mathrm{d}z\right\}, \tag{7}$$

where $c^2 = E/\rho(1-\sigma_{\mathrm{p}}^2)$ is the stiffness coefficient of the film; E is Young's modulus; ρ is the density of the film; and $l_0^2 = h^2/12$. The summation on the right-hand side comprises $d = v$ (vacancies) and $d = i$ (interstitials).

Note that the bending stiffness of the film (the coefficient in front of $\Delta^2\zeta$) depends on its thickness, h, which plays the role of a specific scale parameter for the DD instability of the film. The $\sigma_{\parallel}$ on the left-hand side of (7) takes into account the effect of the isotropic lateral stress arising from the membrane–substrate lattice mismatch and/or defect generation in the near-surface region. We assume that $\sigma_{\parallel} > 0$: the membrane is under known tensile stress. The right-hand side of (7) takes into account the defect-induced bending force normal to the film surface, which arises from the nonuniform defect distribution along the z axis. We neglect the elastic bending nonlinearity of the film in (7), whose effective contribution is smaller than that of the nonlinearity of the deformation-induced drift in (6).

A more complete formulation of the problem should take into account that film bending gives rise to a displacement $\boldsymbol{u}$ in the substrate, which in turn results in an additional term on the right-hand side of (7): $\sigma_{\perp}/\rho h$, where $\sigma_{\perp}$ is the stress normal to the film surface, which originates from the action of the substrate on the film (response of the substrate). One should also take into account the boundary conditions at the film–substrate interface for quasi-Lamb displacement waves in the film and quasi-Rayleigh waves in the substrate [11]. In this formulation of the problem, the response of the substrate can be neglected when

$$\sigma_{\parallel} > \mu_{\mathrm{s}}\left[\frac{\Lambda_{\mathrm{m}}(1-\beta_{\mathrm{s}})}{\pi h}\right], \tag{8}$$

where Λ_{m} is the DD structure period; $\beta_{\mathrm{s}} = c_{\mathrm{t}}^2/c_{\mathrm{l}}^2$; c_{l} and c_{t} are, respectively, the longitudinal and transverse sound velocities in the substrate; and μ_{s} is the shear modulus of the substrate at the film–substrate interface. Condition (8) can be met e.g. when the effective shear modulus at the film–substrate interface approaches zero: $\mu_{\mathrm{s}} \to 0$ [16, 17]. With focus on the conceptual feasibility of describing the main experimental data presented in Section 2, consider the simplest free film model [10], neglecting the response of the substrate.

Equations (1), (6) and (7) then constitute a closed system if $f(z)$ is known and describe the DD instability of a stressed surface membrane containing mobile defects.

5. Increment of growth of the amplitude of surface DD ring structures as a function of their wavenumber (period)

The surface defect density can be represented as

$$N_{\mathrm{d}}(\boldsymbol{r},t) = N_{\mathrm{d}0} + N_{\mathrm{d}1}(\boldsymbol{r},t), \tag{9}$$

where N_{d0} is a spatially uniform term and $N_{d1}(\boldsymbol{r}, t)$ is a spatially nonuniform term in the defect density ($N_{d1}(\boldsymbol{r}, t) \ll N_{d0}$). Linearising (4) and substituting (9), we obtain

$$\frac{\partial N_{d1}}{\partial t} = D_d \Delta N_{d1} - D_d \frac{v\theta_d h}{2kT} N_{d0} \Delta^2 \zeta. \tag{10}$$

Let

$$n_d(\boldsymbol{r}, z, t) = n_{d0} + n_{d1}(\boldsymbol{r}, z, t), \tag{11}$$

where n_{d0} and $n_{d1}(\boldsymbol{r}, z, t)$ are, respectively, a spatially uniform and a spatially nonuniform term in the defect density. It can be shown that, since $h \ll \Lambda_m$ (where Λ_m is the period of the laser-induced structure), the spatially nonuniform z-axis defect distribution resulting from film bending, rapidly adjusts itself to the bending strain distribution along the z axis and is given by

$$n_{d1}(\boldsymbol{r}, z, t) = \frac{2}{h}\left(\frac{h}{2} - z\right) N_{d1}(\boldsymbol{r}, t). \tag{12}$$

Therefore,

$$n_{d1}(z = 0) = -n_{d1}(z = h) = N_{d1}. \tag{12a}$$

Given that strain adiabatically adjusts itself to the defect system, $\partial^2\zeta/\partial t^2 = 0$, and taking into consideration (11)–(12a), we can bring Eqn (7) to the form

$$\Delta^2 \zeta - \frac{1}{l_\parallel^2} \Delta\zeta = -\sum_d A_d \Delta N_{d1}, \tag{13}$$

where $A_d = 2\theta_d/(h l_0^2 \rho c^2)$ and

$$l_\parallel = h\left(\frac{\rho c^2}{12\sigma_\parallel}\right)^{1/2} \tag{14}$$

is a characteristic scale parameter. In what follows, (13) takes into account only one defect species.

Equations (10) and (13) constitute a closed system. Its solution can be written in the form

$$\zeta(r, t) = \zeta_q J_0(qr) \exp(\lambda_q t), \tag{15}$$

$$N_{d1}(r, t) = N_d(q) J_0(qr) \exp(\lambda_q t). \tag{16}$$

Here $J_0(qr)$ is the zeroth-order Bessel function, and ζ_q and $N_d(q)$ are seed amplitudes. Equations (15) and (16) describe a DD ring structure that comprises the surface profile ring structure (15) and defect density (16).

From (13), (15) and (16), we obtain a linear relation between $N_d(q)$ and ζ_q in a DD grating with a wavenumber q:

$$\zeta_q = \eta_d(q) N_d(q), \tag{17}$$

where the DD coupling coefficient in a linear approximation, with the response of the substrate neglected, has the form

$$\eta_d(q) = -\frac{2\theta_d}{h\sigma_\parallel q^2 (q^2 l_\parallel + 1)}. \tag{18}$$

Thus, the seed amplitude of a DD grating is the defect density fluctuation at the initial instant: $N_d(q) \equiv N_d(q, t = 0)$.

Substituting the Fourier transforms (15) and (16) to (10) and using (17) and (18), we find the growth rate for a DD ring structure with a wavenumber q:

$$\lambda_q = D_d q^2 \left(\frac{N_{d0}}{N_{cr}} \frac{1}{1 + l_\parallel^2 q^2} - 1\right), \tag{19}$$

where

$$N_{cr} = \sigma_\parallel \frac{kT}{v\theta_d^2} \tag{20}$$

is the critical defect density.

The $N_{d0}/N_{cr} \equiv \varepsilon$ ratio is a check parameter of DD instability. The function λ_q has a maximum at $q = q_m$, with

$$q_m = \frac{1}{l_\parallel}\left[\left(\frac{N_{d0}}{N_{cr}}\right)^{1/2} - 1\right]^{1/2}. \tag{21}$$

The corresponding period of the dominant DD ring structure, with a wavenumber q_m, takes the form

$$\Lambda_m = \frac{2\pi}{q_m} = \frac{2\pi l_\parallel}{[(N_{d0}/N_{cr})^{1/2} - 1]^{1/2}}, \tag{22}$$

i.e., it is proportional to the film thickness, h [see (14)].

For a grating with $q = q_m$, the maximum growth rate is

$$\lambda_m = D_d q_m^{1/2}\left(\sqrt{N_{d0}/N_{cr}} - 1\right) = \frac{D_d\left(\sqrt{N_{d0}/N_{cr}} - 1\right)^2}{l_\parallel^2} \times \operatorname{sign}\left(\sqrt{N_{d0}/N_{cr}} - 1\right). \tag{23}$$

It follows from (21) and (23) that, above the critical defect density ($\varepsilon = N_{d0}/N_{cr} > 1$), there is a real value of q_m and the growth rate λ_m becomes positive, which corresponds to the formation of a DD ring structure.

6. Comparison of conclusions from the DD theory with experimental data and discussion

The dominant DD ring structure, with a wavenumber q_m, determining the observed surface morphology, has the form of a Lamb static bending wave with a wavelength $\Lambda_m = 2\pi/q_m$, maintained by a self-consistent defect distribution in the membrane. Equations (17) and (18) indicate that, in a DD ring structure, interstitials accumulate ($\theta_d > 0$) at maxima (hillocks) of the surface profile (expanded zones) and vacancies accumulate ($\theta_d < 0$) at minima (depressions) of the surface profile (compressed zones).

At $\sigma_\parallel = 8 \times 10^9$ erg cm^{-3}, $\sigma_p = 0.3$ ($v = 0.571$), $kT = 0.1$ eV ($T \sim 10^3$ K), and $\theta_d = 10^2$ eV, the critical defect density estimated from (20) is $N_{cr} = 8.76 \times 10^{16}$ cm^{-3}. Figure 4 shows the growth rate $\lambda_q = \lambda(q)$ evaluated from (19) with the following parameters: $h = 2 \times 10^{-4}$ cm, $\rho c^2 = 7 \times 10^{11}$ erg cm^{-3}, $\sigma_\parallel = 10^{10}$ erg cm^{-3}, $D_d = 10^{-6}$ cm^2 s^{-1}, and $N_{d0}/N_{cr} = \varepsilon = 3$ or $\varepsilon = 30$. It is seen that, at a sufficiently high defect density, above the critical level, the growth rate has a maximum at $\Lambda_m \sim 14$ μm, which corresponds to the measured period of the ring structure (Fig.3).

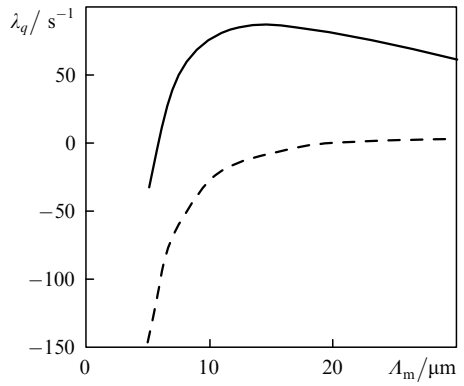

Figure 4. Increment of growth of the surface ring structure amplitude, λ_q, as a function of Λ_m at $N_{q0}/N_c \equiv \varepsilon = 3$ (dashed line) and $\varepsilon = 30$ (solid line). The curves were calculated using relation (19) at the parameters specified in Section 6.

It follows from Fig. 3 that the Fourier spectrum of the surface profile after exposure should contain the first to fourth harmonics in the low-frequency region (Fig. 5). At the same time, relations (15) and (16) predict the formation of a ring structure containing one radial harmonic. To describe the observed surface profile, represented in Figs 2 and 4, one should take into account the possible generation of higher DD ring harmonics. As shown earlier [14], three-wave interactions of DD waves with collinear wave vectors lead to the generation of the second and cascade third DD harmonics. The generation of the second to fourth DD ring harmonics can be analysed in a similar manner. Figure 6 shows a surface profile obtained by simulation using a superposition of the first to fourth harmonics according to the relation

$$\zeta(x) = -(1.7J_0(x) + J_0(2x + 2.5) + 1.2J_0(3x + 2) + 0.9J_0(4x + 4)), \quad (24)$$

where x is the longitudinal coordinate of the surface profile.

The amplitudes of the harmonics in (24) were selected as follows: Because the two-dimensional Fourier transform of a radial function reduces to the zeroth-order radial Hankel transformation, the amplitudes of the first four harmonics in (24) are equal to those in the experimental spectrum in Fig. 5

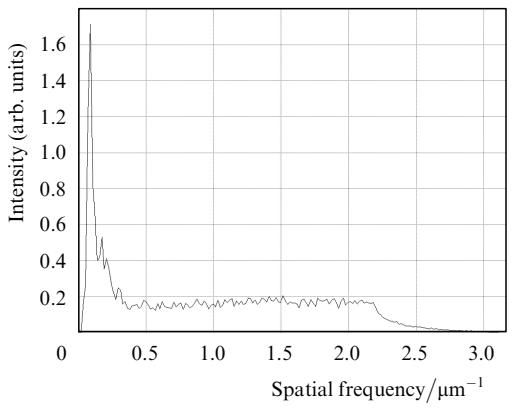

Figure 5. Radial Fourier transform of the measured surface profile after laser exposure (the data are discussed in Section 6).

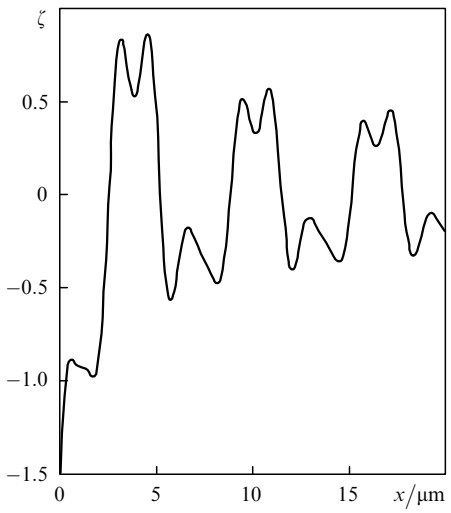

Figure 6. Simulation of the surface profile after exposure with a superposition of the first to fourth harmonics of a ring structure according to the relation $\zeta(x) = -(J_0(x) + J_0(2x+2.5) + J_0(3x+2) + J_0(4x+4))$. The amplitudes of the harmonics were selected with allowance for the spectral amplitudes of the corresponding harmonics in the spectrum presented in Fig. 5.

multiplied by one, two, three, and four (the phases of the harmonics are zero). Nonzero phases of the harmonics in (24) were introduced in an arbitrary manner in order to better represent the observed surface profile shown in Fig. 3. Equation (24) takes into account that, with nonlinear DD interactions, the amplitudes of higher harmonics may exceed those of lower harmonics [14]. Moreover, the direction of the z axis in (24) was changed to the opposite [the z axis is directed upwards and the surface profile is $z(x) = \zeta(x)$]. This is reflected by the change of sign in (18). In addition, we take $\eta_d(q) = 1$. The positive defect – bending coupling coefficient [$\eta_d(q) > 0$] corresponds to the predominant role of surface interstitials ($\theta_d > 0$) in DD instability. The superposition of four harmonics in (24) is seen to qualitatively reproduce the key features of the observed surface profile: the dip in the centre of the laser spot, strong peaks whose amplitude decreases with increasing distance from the centre, the relatively large separation between the peaks (as compared to their width) and, finally, the splitting of each strong peak into two components.

7. Conclusions

We studied solid-state laser modification of the surface of PbSe semiconductor films and identified surface self-organisation at photon energies above the band gap of the semiconductor. Experimental data were used to construct a model for defect – deformation instability developing on the surface of an epitaxial film through strain-induced drift of laser-induced point defects. The model is capable of qualitatively describing the observed surface morphology and predicting the surface profile in laser modification experiments.

Acknowledgements. This work was supported by the RF Ministry of Education and Science through the Development of the Scientific Potential of Higher Education Institutions Programme (Project No. 2.1.1/466). We are grateful to H. Zogg (ETH Zurich) for kindly providing the

lead selenide films and for his continuous interest in this research.

References

1. Mukherjee S., Li D., Kar A.G.J., Shi Z. *Transworld Research Network* (Kerala, India, 2010) p. 88.
2. Abtin L., Springholz G., Holy V. *Phys. Rev. Lett.*, **97**, 266103 (2006).
3. Zimin S.P., Gorlachev E.S., Amirov I.I., Zogg H. *J. Phys. D: Appl. Phys.*, **42**, 165205 (2009).
4. Grekov Yu.B., Semikolenova N.A., Shlyakhov T.A. *Fiz. Tekh. Poluprovodn.,* **31** (8), 990 (1997).
5. Plyatsko S.V. *Fiz. Tekh. Poluprovodn.*, **32** (3), 257 (1998).
6. Zimin S.P., Bogoyavlenskaya E.A., Gorlachev E.S., Naumov V.V., Zimin D.S., Zogg H. *Semicond. Sci. Technol.*, **22**, 1317 (2007).
7. Prokoshev V.G., Galkin A.F., Klimovskii I.I., Danilov S.Yu., Abramov D.V., Arakelyan S.M. *Kvantovaya Elektron.*, **25**, 337 (1998) [*Quantum Electron.*, **28**, 326 (1998)].
8. Prokoshev V.G., Klimovskii I.I., Galkin A.F., Abramov D.V., Arakelyan S.M. *Izv. Akad. Nauk, Ser. Fiz.*, **661**, 1560 (1997).
9. Bagaev S.N., Kucherik A.O., Abramov D.V., Arakelyan S.M., Prokoshev V.G., Klimovskii I.I. *Dokl. Akad. Nauk*, **395** (2), 183 (2004).
10. Emel'yanov V.I., in *Nelineinye volny* (Nonlinear Waves) (Moscow: Nauka, 1989) p. 198.
11. Emel'yanov V.I. *Kvantovaya Elektron.*, **28** (1), 2 (1999) [*Quantum Electron.*, **29** (7), 561 (1999)].
12. Zogg H., Maissen C., Blunier S., Teodoropol S., Overney R.M., Richmond T., Tomm J.W. *Semicond. Sci. Technol.*, **8** (1S), S337 (1993).
13. Viktorov I.A. *Zvukovye poverkhnostnye volny v tverdykh telakh* (Surface Acoustic Waves in Solids) (Moscow: Nauka, 1981).
14. Emel'yanov V.I., Seval'nev D.M. *Kvantovaya Elektron.*, **39** (7), 678 (2009) [*Quantum Electron.*, **39** (7), 678 (2009)].
15. Landau L.D., Lifshitz E.M. *Theory of Elasticity* (Oxford: Pergamon, 1970; Moscow: Nauka, 1965).
16. Bottani C.E., Yakona M. *J. Phys.: Condens. Matter.*, **I**, 8337 (1989).
17. Dodson B.W., Tsao J.Y. *Appl. Phys. Lett.*, **51**, 1325 (1987).